communications biology

Article

https://doi.org/10.1038/s42003-024-07024-5

Overexpression of USP35 enhances the protective effect of hUC-MSCs and their extracellular vesicles in oxygen-glucose deprivation/reperfusion-induced SH-SY5Y cells via stabilizing FUNDC1

Check for updates

Shuo Wang[1], Xigong Li[1], Tianjiao Wang[2], Zeyu Sun[1], Erwei Feng[1] & Yongming Jin[1]

Ischemia-reperfusion (IR) injury is associated with neurological disorders such as stroke. The therapeutic potential of human umbilical cord mesenchymal stem cells (hUC-MSCs) and their secreted extracellular vesicles (EVs) in alleviating IR injury across various cell types including neuronal cells has been documented. However, the underlying mechanisms through which hUC-MSCs and hUC-MSC-EVs protect neuronal cells from IR-triggered damage are not well understood. In this study, we co-cultured SH-SY5Y neuroblastoma cells with hUC-MSCs or hUC-MSC-EVs and subjected them to oxygen-glucose deprivation/reperfusion (OGD/R) treatment. Our findings indicate that both hUC-MSCs and hUC-MSC-EVs significantly improved viability, reduced apoptosis, promoted autophagy of OGD/R-induced SH-SY5Y cells, and decreased mitochondrial reactive oxygen species levels within them. Furthermore, the neuroprotective effect of hUC-MSCs and hUC-MSC-EVs in OGD/R-induced SH-SY5Y cells was enhanced by overexpressing USP35, a deubiquitinase. Mechanistically, USP35 interacted with and stabilized FUNDC1, a positive regulator of mitochondrial metabolism. Knockdown of FUNDC1 in USP35-overexpressing hUC-MSCs and their secreted EVs eliminated the augmented neuroprotective function induced by excess USP35. In conclusion, these findings underscore the crucial role of USP35 in enhancing the neuroprotective function of hUC-MSCs and their secreted EVs, achieved through the stabilization of FUNDC1 in OGD/R-induced SH-SY5Y cells.

Ischemic stroke stands as one of the cardiovascular diseases globally, characterized by significant morbidity and mortality[1,2]. After a period of prolonged ischemia caused by stroke, the restoration of blood flow triggers inflammation and an excessive generation of reactive oxygen species (ROS). This harmful cascade results in neuronal cell death and subsequent brain damage, a phenomenon known as cerebral ischemia-reperfusion (IR) injury (CIRI)[1,3,4]. Within CIRI, multiple programmed cell death (PCD) pathways are involved, including apoptosis, necroptosis, pyroptosis, and autophagy[4,5]. These pathways involve a range of cell death factors, such as apoptosis regulators like BCL-2[6,7] and Caspase 3[7], the inflammation-related cytokine TNF[8,9], as well as autophagy mediators ULK1 and LC3[10,11]. Given that neuronal cell death is a pivotal outcome of CIRI, targeting and inhibiting these PCD pathways responsible for neuronal death emerge as crucial therapeutic avenues, which may potentially enhance the prognosis and treatment of ischemic stroke.

Human umbilical cord mesenchymal stem cells (hUC-MSCs) hold promise as a foundation for stem cell-based therapies due to their rapid self-renewal capacity, pluripotency, simple collection procedure, and relatively easy accessibility[12,13]. However, the tumorigenic tendencies of these cells, along with ethical constraints related to cell therapy, impede the widespread adoption of hUC-MSCs clinically[12,14]. Consequently, researchers are exploring alternatives to hUC-MSCs, among which extracellular vesicles (EVs) derived from hUC-MSCs (hUC-MSC-EVs) have emerged. These EVs exhibit similar therapeutic effects in diverse diseases, including

[1]Department of Orthopedics Surgery, The First Affiliated Hospital, Zhejiang University School of Medicine, Hangzhou, Zhejiang, 310006, People's Republic of China. [2]Zhejiang Provincial Center for Disease Control and Prevention, Hangzhou, Zhejiang, 310051, People's Republic of China. e-mail: 1320182@zju.edu.cn

injury-associated kidney diseases[15,16], inflammatory bowel disease[17,18], and myocardial damage[19,20]. Notably, hUC-MSC-EVs also demonstrate the ability to curb pyroptosis and ferroptosis in instances of ischemic reperfusion (IR)-induced cardiac, renal, and neuronal injuries[19,21,22]. Despite these advancements, the precise mechanisms through which hUC-MSCs and hUC-MSC-EVs mitigate damages induced by IR remain incompletely elucidated.

Ubiquitination stands as a crucial posttranslational modification regulating the stability and functionality of target proteins. It's estimated that the ubiquitin-proteasome system is accountable for over 80% of protein degradation within cells[23]. This process involves the E3 ubiquitin ligase family, appending ubiquitin modifications and comprised of numerous members with distinct substrate specificity. In contrast, deubiquitinases (DUBs) are responsible for the removal of ubiquitin modifications from their target proteins. Within the human system, more than a hundred DUBs have been identified, and categorized into seven families based on their structural traits[24,25]. Among these families, the ubiquitin-specific proteases (USPs) constitute the largest group[24,26]. Out of these, 54 share the conserved S1 ubiquitin-binding site. However, their substrate-interacting domains are not uniform, leading to a diverse range of interactions with target proteins[26,27].

FUNDC1, a mitochondrial outer membrane receptor exhibiting a high degree of conservation across species, holds a crucial role in initiating mitochondrial autophagy, commonly referred to as mitophagy[28]. Normally, FUNDC1 undergoes phosphorylation at Tyr18. Yet, oxidative stress diminishes the activity of the tyrosine kinase responsible for phosphorylating FUNDC1. This leads to a notable rise in the affinity of the LC3-interacting region within FUNDC1. Consequently, LC3 is recruited to mitochondria, effectively initiating the process of mitophagy[28]. In conditions where mitochondria are exposed to ROS-induced stress, mitophagosomes are formed. These structures serve to sequester oxidative phosphorylation enzymes, such as cytochrome C, thereby preventing their release into the cytoplasm. This action curbs subsequent cell apoptosis, thereby contributing to the mitigation of CIRI[29]. The regulation of FUNDC1's stability and degradation involves the intervention of E3 ubiquitin ligases, particularly MARCH5. This ligase facilitates the degradation of FUNDC1, thereby impeding the progression of autophagy[30]. Nevertheless, whether the ubiquitination and stability of FUNDC1 are controlled by DUBs remains an area necessitating further investigation, along with the underlying mechanisms governing this process.

In this study, we aimed to validate the neuroprotective capabilities of both hUC-MSCs and hUC-MSC-EVs using SH-SY5Y neuroblastoma cells subjected to oxygen-glucose deprivation/reperfusion (OGD/R). A comprehensive screening involving 40 USPs was conducted to identify potential regulators of FUNDC1 stability. Through this screening, USP35 emerged as a prominent factor contributing to the stabilization of FUNDC1. Subsequent experiments provided insight into how overexpression of USP35 further bolstered hUC-MSCs and hUC-MSC-EVs in promoting the survival of SH-SY5Y cells under OGD/R conditions. Mechanistically, it was discovered that USP35 interacted with FUNDC1 and executed deubiquitination processes, thereby enhancing the stability of FUNDC1. Critically, the intensified neuroprotective effect triggered by excessive USP35 was abolished upon the knockdown of FUNDC1. These observations uncover the previously unrecognized role of USP35 in enhancing the protective capacity of both hUC-MSCs and hUC-MSC-EVs in alleviating IR-triggered injury to neuronal cells.

Results

Characterization of hUC-MSC and hUC-MSC-EV

To elucidate the biological function of hUC-MSC and hUC-MSC-EV, we initiated by obtaining hUC-MSCs and conducting a comprehensive examination of their characteristics. We observed that these cells exhibited a distinctive spindle-shaped morphology (Fig. 1A). Moreover, flow cytometry analysis revealed that these cells lacked the expression of hematopoietic cell markers such as CD14, CD19, CD34, CD45, or HLA-DR. However, they prominently expressed MSC markers, including CD29, CD44, CD73, CD90, and CD105[31,32] (Fig. 1B). To further evaluate the pluripotency of these cells, we induced them to differentiate into osteocytes, chondrocytes, and adipocytes by employing distinct culture media. Remarkably, these hUC-MSCs exhibited successful differentiation into the indicated cell types (Fig. 1C). This substantiated and solidified their characterization as hUC-MSCs. We then performed EV isolation and purification from these hUC-MSCs. Western blot results showed that these EVs were enriched in the expression of EV markers CD9, CD81, and CD63[33] (Fig. 1D). Furthermore, transmission electron microscopy (TEM) and nanoparticle tracking analysis (NTA) indicated that these EVs exhibited typical EV morphology, and their diameter ranged from 50 ~ 150 nm (Fig. 1E and F). These findings collectively provided a concrete confirmation of the distinctive characteristics of hUC-MSCs and the EVs they secreted.

hUC-MSC and hUC-MSC-EV improved viability, inhibited apoptosis, reduced ROS level, and enhanced autophagy in SH-SY5Y OGD/R cells

To replicate the cellular damage induced by CIRI, we employed the SH-SY5Y neuroblastoma cell line to establish an in vitro OGD/reperfusion (OGD/R) model as previously[34–36]. The duration of reperfusion was varied to optimize the OGD/R model. The results from MTT staining indicated an inverse relationship between increased reperfusion time and the viability of SH-SY5Y cells subjected to OGD (Fig. S1A). In line with this, the level of apoptosis within these cells escalated as the reperfusion time was extended (Fig. S1B-C). Given that a 3-hour reperfusion period was adequate to induce the phenotypes of IR, this particular condition was adopted for subsequent experiments. Consequently, these cells were subsequently referred to as SH-SY5Y OGD/R cells.

To evaluate the impact of hUC-MSCs and hUC-MSC-EVs on SH-SY5Y OGD/R cells, we initiated by coculturing SH-SY5Y OGD/R cells with hUC-MSCs. MTT assay results demonstrated a significant increase in the viability of SH-SY5Y OGD/R cells upon coculture with hUC-MSCs (Fig. 2A). Notably, the introduction of GW4869, an inhibitor of EV secretion[37], effectively counteracted the viability-enhancing effect of hUC-MSCs on cocultured SH-SY5Y OGD/R cells (Fig. 2A). This indicated the potential involvement of hUC-MSC-EVs in mediating the viability-promoting function of hUC-MSCs. Supporting this, we observed that hUC-MSC-EVs displayed similar effects to hUC-MSCs on the viability of SH-SY5Y OGD/R cells (Fig. 2A).

We proceeded to assess the impact of hUC-MSCs and hUC-MSC-EVs on the apoptosis of SH-SY5Y OGD/R cells. Annexin V/PI staining revealed a significant reduction in the apoptosis of SH-SY5Y OGD/R cells upon coculture with hUC-MSCs. This anti-apoptotic effect was attenuated by GW4869-mediated inhibition of EV production but was replicated by hUC-MSC-EVs (Fig. 2B and C). This indicated a resemblance between hUC-MSC-EVs and hUC-MSCs in reducing the apoptosis of SH-SY5Y OGD/R cells. To further validate the uptake of hUC-MSC-EVs by these cells, we conducted a CFSE-labeled EV tracing assay, which confirmed the efficient absorption of hUC-MSC-EVs by SH-SY5Y OGD/R cells. Additionally, the anti-apoptotic function of these EVs was observed to persist for at least 48 hours (Fig. S2A-C).

To find out whether ROS levels were changed by hUC-MSC or hUC-MSC-EV, we examined the mitochondria of SH-SY5Y OGD/R cells. TEM results indicated that coculturing SH-SY5Y OGD/R cells with hUC-MSCs led to a significant increase in the number of mitochondria, with their morphology closely resembling normal mitochondria (Fig. 2D). However, this effect was impaired by GW4869 treatment, as the mitochondrial morphology was abnormal (Fig. 2D). Similarly, hUC-MSC-EVs were observed to improve both the number and morphology of mitochondria in SH-SY5Y OGD/R cells (Fig. 2D). This suggests that hUC-MSCs might regulate mitochondria metabolism in SH-SY5Y OGD/R cells through their secreted EVs. In line with this, we found that coculturing SH-SY5Y OGD/R cells with hUC-MSCs or hUC-MSC-EVs substantially improved the disrupted mitochondrial membrane potential of SH-SY5Y OGD/R cells, as evidenced by JC-1 staining results (Fig. 2E and F). Furthermore, DCF

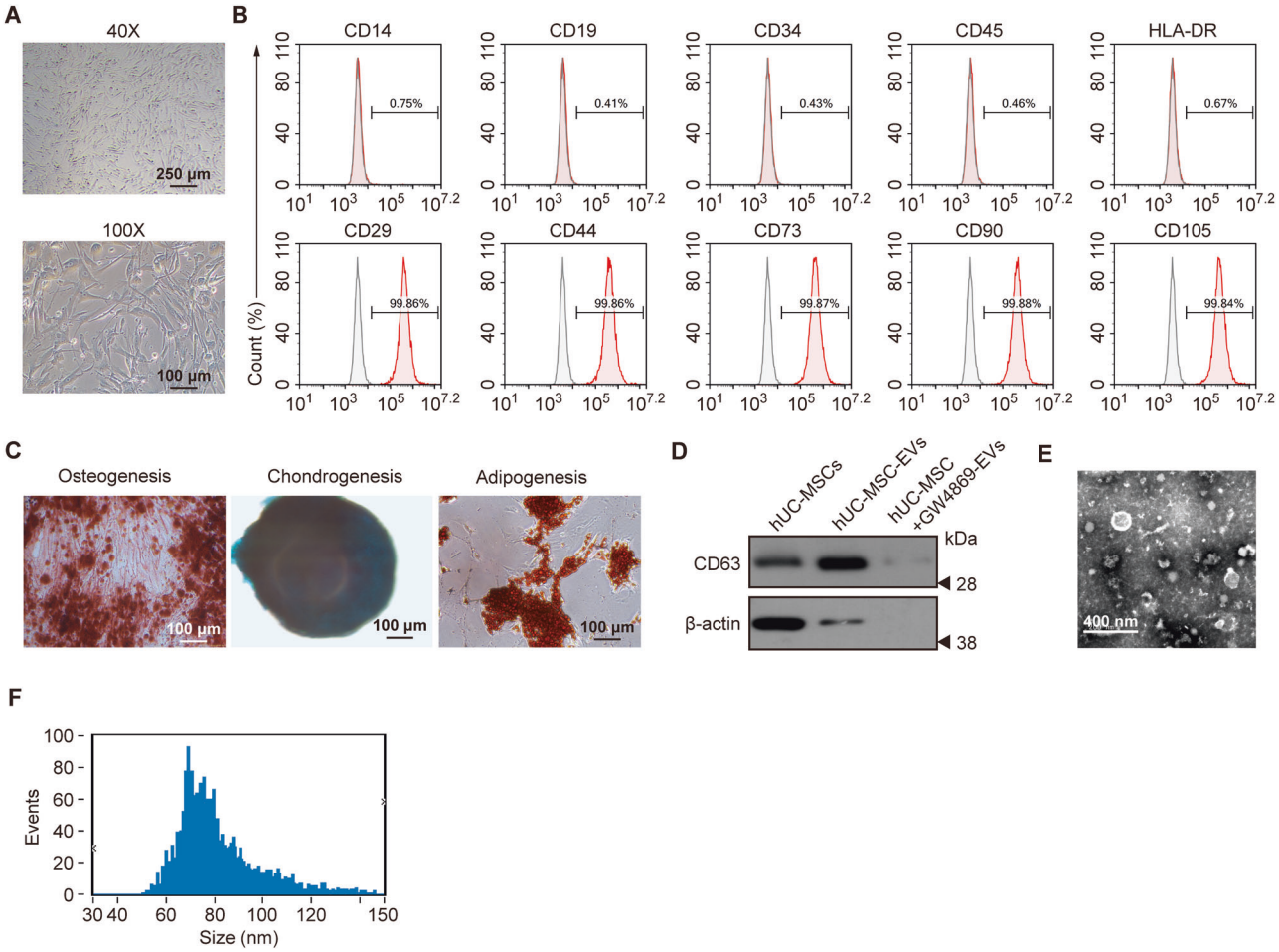

Fig. 1 | Characterization of hUC-MSC and hUC-MSC-EV. A The morphology of hUC-MSCs as observed under a bright-field microscope. **B** Flow cytometry results depicting the expression of designated cell surface markers. **C** Staining results for alizarin red (left), alcian blue (middle), and oil red O (right), revealing the successful differentiation of hUC-MSCs into osteocytes (left), chondrocytes (middle), and adipocytes (right), respectively. **D** Western blot analysis demonstrating the abundant presence of EV markers CD63 in the purified EVs and the high efficiency of GW4869 in blocking EV production by hUC-MSCs. **E** TEM images illustrating the structural characteristics of the purified EVs. **F** NTA results depicting the size distribution of the purified EVs.

staining data indicated that both hUC-MSCs and hUC-MSC-EVs exhibited a similar effect in reducing ROS levels within SH-SY5Y OGD/R cells (Fig. 2G and H). However, this effect was partially blocked by GW4869 treatment (Fig. 2G and H).

Given the established connection between increased ROS levels and apoptosis as well as autophagy[38–41], we proceeded to assess the expression of markers associated with apoptosis and autophagy using Western blot analysis. We noted that the expression of FUNDC1 and Cyt C within SH-SY5Y OGD/R cells was significantly upregulated and downregulated, respectively, upon coculture with hUC-MSCs or hUC-MSC-EVs. This effect was abolished by GW4869 treatment, suggesting that mitophagy within SH-SY5Y OGD/R cells was enhanced by hUC-MSCs or hUC-MSC-EVs (Fig. 3A and B). Consistently, both hUC-MSCs and hUC-MSC-EVs substantially elevated the expression of Beclin-1 and LC3 II, markers indicating autophagy activation, and significantly reduced the expression of autophagy substrate p62 within cocultured SH-SY5Y OGD/R cells. This effect was also abolished by GW4869 treatment (Fig. 3A and B). Furthermore, the expression of the anti-apoptotic protein BCL2 was increased, while the levels of pro-apoptotic factors BAX and cleaved Caspase 3/9 were reduced in cocultured SH-SY5Y OGD/R cells by both hUC-MSCs and hUC-MSC-EVs. However, this effect was not observed in SH-SY5Y OGD/R cells treated with GW4869 (Fig. 3A and B). Together, these findings suggest that both hUC-MSCs and hUC-MSC-EVs are effective in enhancing viability, reducing apoptosis, lowering ROS levels, and promoting autophagy within SH-SY5Y OGD/R cells.

USP35 interacted with and stabilized FUNDC1 by repressing its ubiquitination

To gain insights into the mechanism underlying the protective effects of hUC-MSCs and hUC-MSC-EVs on SH-SY5Y OGD/R cells, we investigated their influence on FUNDC1, a key protein involved in mitophagy initiation. Notably, the expression of FUNDC1 in SH-SY5Y OGD/R cells was significantly increased upon treatment with hUC-MSCs or hUC-MSC-EVs. Given the critical role of the ubiquitin system in regulating FUNDC1 stability, a screening of 40 USPs that could potentially influence FUNDC1 ubiquitination was performed. This screening employed stable HEK293T cells expressing luciferase-conjugated FUNDC1 and individually overexpressed each USP. The luciferase activity assay revealed that the overexpression of USP19 or USP35 resulted in the top two strongest luciferase signals in HEK293T cells (Fig. 4A). This finding suggested that both USP19 and USP35 might function as potent stabilizers of FUNDC1. Because the role of USP19 in mitochondrial FUNDC1 has been reported in another context[42], the subsequent investigations focused on USP35 to understand its impact on FUNDC1 metabolism. Supporting the notion of USP35's role in stabilizing FUNDC1 from the luciferase assay, the knockdown of USP35 was observed to substantially decrease the level of FUNDC1 in HEK293T cells (Fig. 4B). The shRNA sequence with higher efficiency in

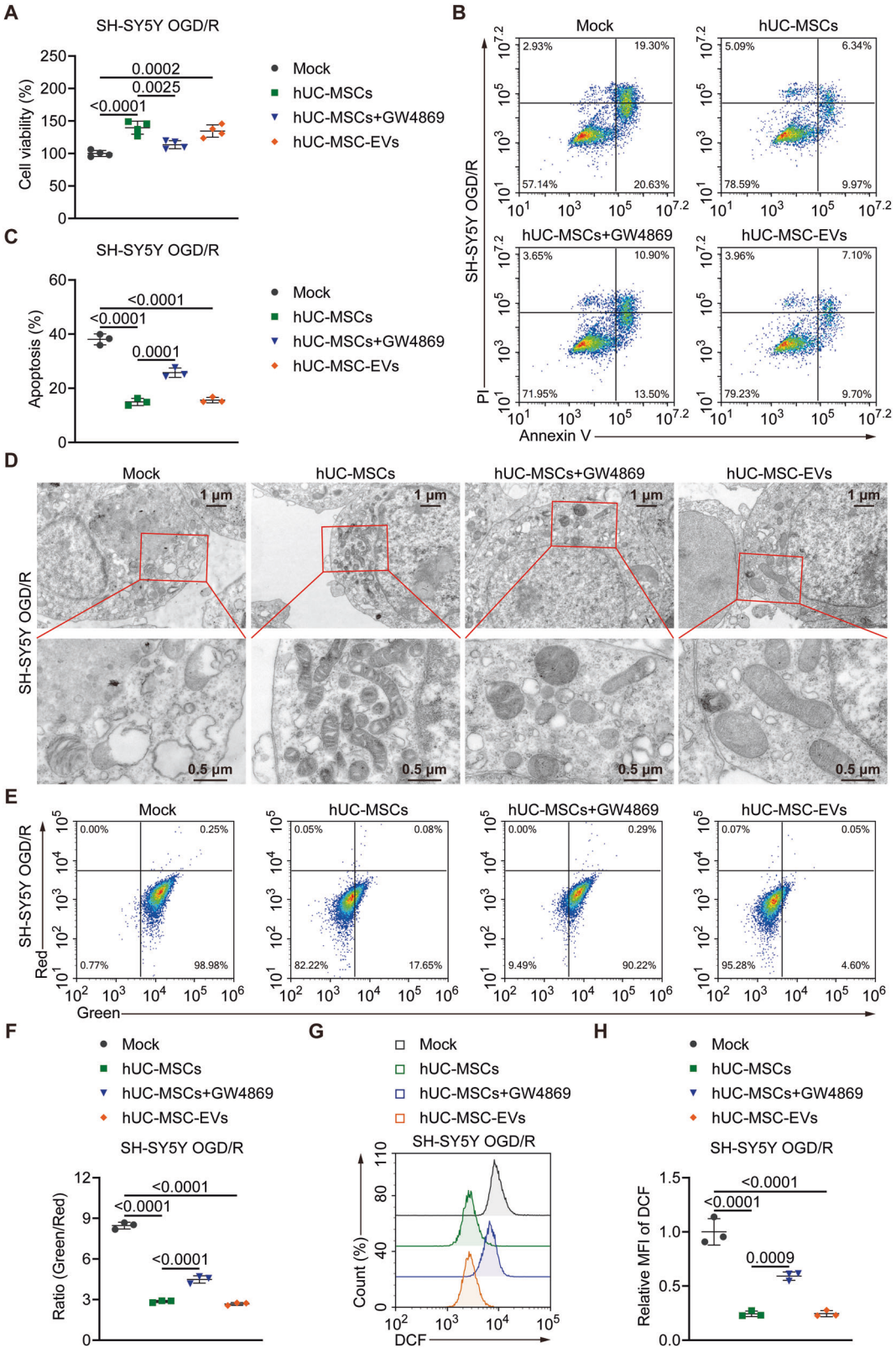

repressing USP35 expression, shUSP35-1, was selected for further experiments.

To explore whether FUNDC1 stability in SH-SY5Y cells is indeed regulated by the ubiquitin system, a treatment involving the protein synthesis inhibitor CHX and the proteasome inhibitor MG132 was employed. This strategy aimed to inhibit ubiquitin-dependent protein degradation. Western blot results demonstrated that the protein levels of FUNDC1 increased in a dose-dependent manner upon MG132 treatment, indicating the importance of ubiquitination in regulating FUNDC1 stability in SH-SY5Y cells (Fig. 4C). Furthermore, the involvement of USP35 in the stabilization of FUNDC1 within SH-SY5Y cells was verified, and the interaction between the two proteins was explored. This was achieved by

Fig. 2 | hUC-MSC and hUC-MSC-EV improved viability, inhibited apoptosis, reduced ROS level, and enhanced autophagy in SH-SY5Y OGD/R cells. A MTT staining results indicated that both hUC-MSCs and hUC-MSC-EVs enhanced the viability of cocultured SH-SY5Y OGD/R cells. However, treatment with GW4869 compromised this viability-promoting effect of hUC-MSCs. **B** Annexin V/PI staining data demonstrated that hUC-MSCs and hUC-MSC-EVs decreased the apoptosis of cocultured SH-SY5Y OGD/R cells. Nonetheless, the anti-apoptotic role of hUC-MSCs was weakened in the presence of GW4869. **C** Quantitative analysis of the Annexin V/PI staining data. **D** TEM images depicting the morphological features of mitochondria in SH-SY5Y OGD/R cells treated with different conditions. **E** JC-1 staining results, indicating that hUC-MSC-EVs exhibited a similar effect to hUC-MSCs in restoring the dysregulated mitochondrial membrane potential in cocultured SH-SY5Y OGD/R cells. However, this effect of hUC-MSCs was also dampened by GW4869. **F** Quantitative assessment of the JC-1 staining outcomes. **G** DCF staining outcomes revealed that the levels of ROS in SH-SY5Y OGD/R cells were reduced upon coculture with hUC-MSCs or hUC-MSC-EVs. The ROS-reducing function of hUC-MSCs was compromised by GW4869 treatment as well. **H** Quantitative analysis of the DCF staining data.

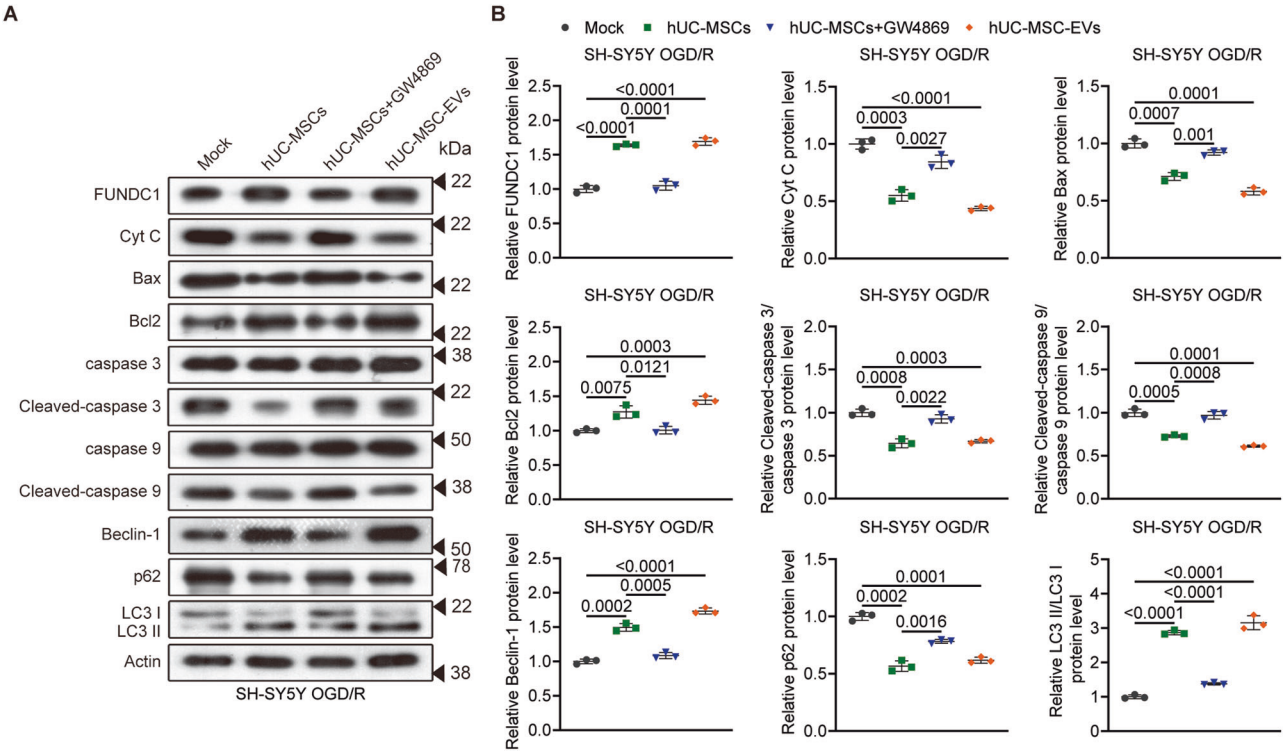

Fig. 3 | hUC-MSC and hUC-MSC-EV altered the expression of proteins correlated to apoptosis, ROS production, and autophagy in SH-SY5Y OGD/R. A Western blot analysis revealed that coculture with hUC-MSCs or hUC-MSC-EVs increased the levels of FUNDC1, Bcl2, Beclin-1, and the LC3 II/I ratio, while decreasing the levels of Cyt C, Bax, cleaved-Caspase 3/9, and p62 in SH-SY5Y OGD/R cells. In contrast, hUC-MSCs treated with GW4869 did not exhibit such effects. **B** Quantitative assessment of the Western blot results.

overexpressing HA-USP35 and Flag-FUNDC1 in SH-SY5Y cells, followed by co-immunoprecipitation (co-IP) assays. The data from these assays indicated a direct interaction between USP35 and FUNDC1 within the cells (Fig. 4D). As USP35 is a DUB responsible for removing ubiquitin modifications from target proteins, His-tagged ubiquitin was introduced into FUNDC1-overexpressing SH-SY5Y cells. Subsequent co-IP results showed that the knockdown of USP35 led to a significant increase in the ubiquitination level of FUNDC1, while the overexpression of USP35 remarkably reduced the ubiquitination of FUNDC1 in SH-SY5Y cells (Fig. 4E and F). Moreover, USP35 knockdown accelerated FUNDC1 degradation, while excessive USP35 inhibited FUNDC1 degradation in these cells (Fig. 4G and H). These findings demonstrate that USP35 stabilizes FUNDC1 by removing its ubiquitination.

Overexpression of USP35 enhanced the protective effect of hUC-MSC and hUC-MSC-EV on SH-SY5Y cells with OGD/R treatment

We then investigated whether USP35 overexpression could potentiate the function of hUC-MSC and hUC-MSC-EV in alleviating apoptosis and reducing ROS stress in SH-SY5Y OGD/R cells. MTT staining data indicated that USP35 overexpression led to a significant enhancement of the viability-promoting effect of hUC-MSCs on SH-SY5Y OGD/R cells (Fig. 5A). Interestingly, although hUC-MSCs overexpressing USP35 generated EVs with elevated levels of USP35, leading to increased USP35 expression in cocultured SH-SY5Y cells (Fig. S3A-C), and these hUC-MSC-EVs displayed effects comparable to hUC-MSCs on SH-SY5Y OGD/R cells, the inhibition of EV production by GW4869 only partially attenuated the viability-promoting function of hUC-MSCs on cocultured SH-SY5Y OGD/R cells. This observation suggests that hUC-MSCs may employ additional mechanisms beyond EV secretion to fulfill this function (Fig. 5A). Consistently, excessive USP35 amplified the anti-apoptotic effect of hUC-MSCs and hUC-MSC-EVs on SH-SY5Y OGD/R cells. Notably, the treatment of GW4869 mitigated this enhanced function of hUC-MSCs (Fig. 5B and C). Moreover, TEM results revealed that USP35 overexpression in hUC-MSCs and hUC-MSC-EVs led to an increased number of mitochondria and improved mitochondrial morphology within cocultured SH-SY5Y OGD/R cells (Fig. 5D). Furthermore, JC-1 and DCF staining results demonstrated that USP35-overexpressing hUC-MSCs and hUC-MSC-EVs exhibited superior efficacy in restoring the abnormal mitochondrial membrane potential and reducing ROS levels in cocultured SH-SY5Y OGD/R cells, compared to control hUC-MSCs and hUC-MSC-EVs. Notably, these protective effects were attenuated upon treatment with GW4869 (Fig. 5E-H).

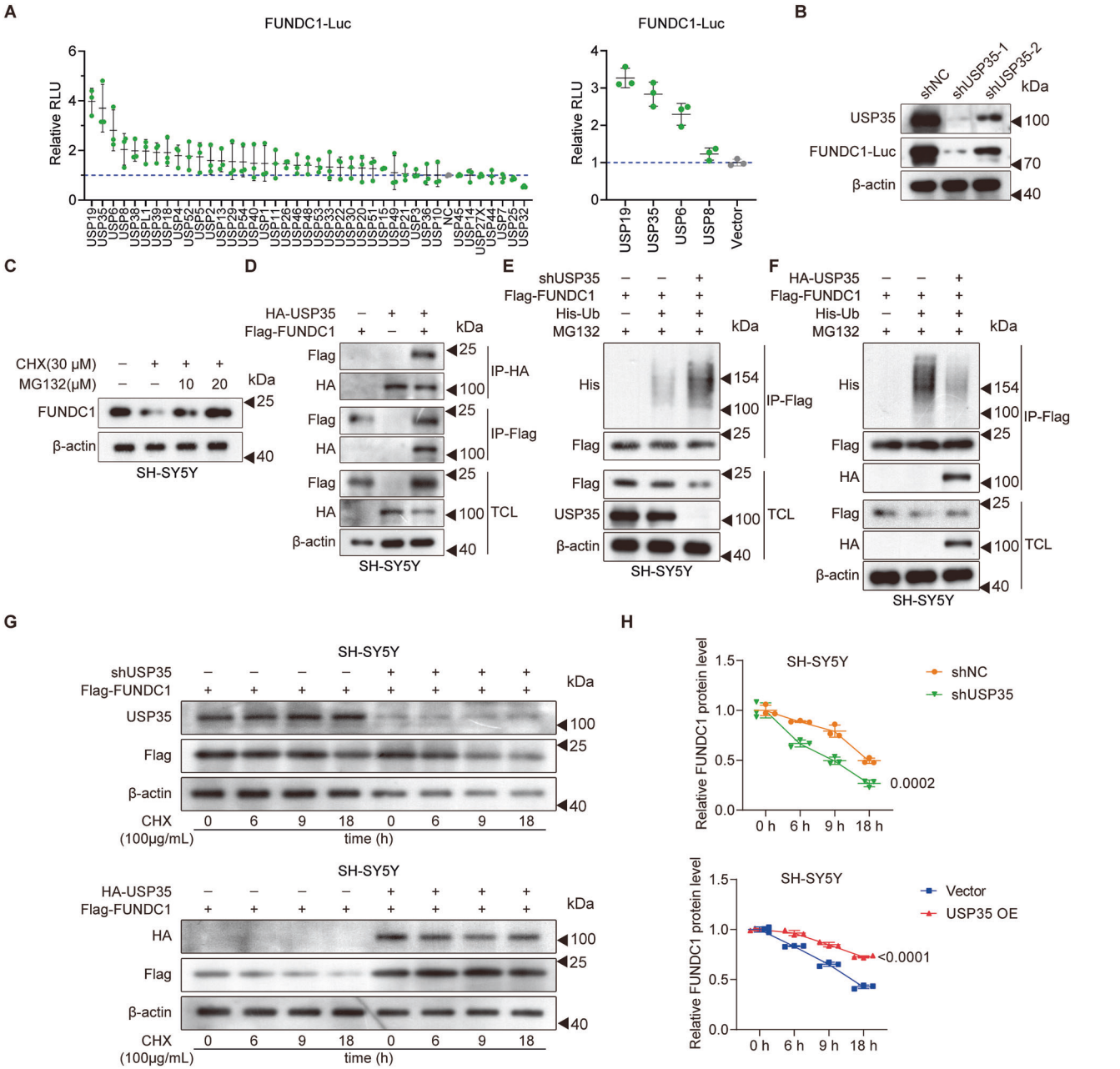

Fig. 4 | USP35 interacted with and deubiquitinated FUNDC1 in SH-SY5Y cells. **A** Normalized luciferase activity assay data demonstrated the impact of overexpressing the indicated USPs on the expression of FUNDC1 in HEK293T cells. **B** Western blot analysis revealed that knockdown of USP35 led to a significant reduction in the expression of luciferase-conjugated FUNDC1 (FUNDC1-Luc). **C** Western blot results indicated that treatment with increasing doses of MG132 led to a dose-dependent increase in FUNDC1 levels in SH-SY5Y cells. **D** Co-IP data indicated the interaction between HA-USP35 and Flag-FUNDC1 in SH-SY5Y cells. **E** Co-IP results revealed that deficiency of USP35 resulted in elevated levels of ubiquitinated FUNDC1 in SH-SY5Y cells. **F** Co-IP findings showed that excessive USP35 decreased the ubiquitination of FUNDC1 in SH-SY5Y cells. **G** Western blot data demonstrated that knockdown of USP35 accelerated the degradation of FUNDC1, while overexpression of USP35 had the opposite effect. **H** Quantitative analysis of the data presented in **G**.

By contrast, hUC-MSC-EVs that overexpress a mutant USP35, which lacks its catalytic function, exert a similar influence as control hUC-MSC-EVs on the viability, apoptosis, and ROS levels of the cocultured SH-SY5Y OGD/R cells (Fig. S4A-E). This indicates that the catalytic domain is required for USP35 to fulfill its protective function in this context.

At the molecular level, the SH-SY5Y OGD/R cells cocultured with USP35-overexpressing hUC-MSCs or hUC-MSC-EVs exhibited elevated levels of FUNDC1, Bcl2, Beclin-1, and LCII, along with decreased levels of cytoplasmic Cyt C, BAX, cleaved-Caspase 3/9, and p62, when compared to cells cocultured with control hUC-MSCs or hUC-MSC-EVs. The alterations in the expression of these proteins were also partially mitigated upon treatment with GW4869 (Fig. 6A and B). Collectively, these findings suggest that excessive USP35 enhances the capacity of hUC-MSCs and hUC-MSC-EVs to reduce apoptosis and ROS stress in cocultured SH-SY5Y OGD/R cells.

Knockdown of FUNDC1 abolished the effects of excessive USP35 in strengthening the protective roles of hUC-MSC and hUC-MSC-EV on SH-SY5Y OGD/R

Considering that USP35 influences the stability of FUNDC1, we proceeded to investigate whether FUNDC1 is a prerequisite for the role of USP35 in hUC-MSCs and their secreted EVs in relation to SH-SY5Y OGD/R cells.

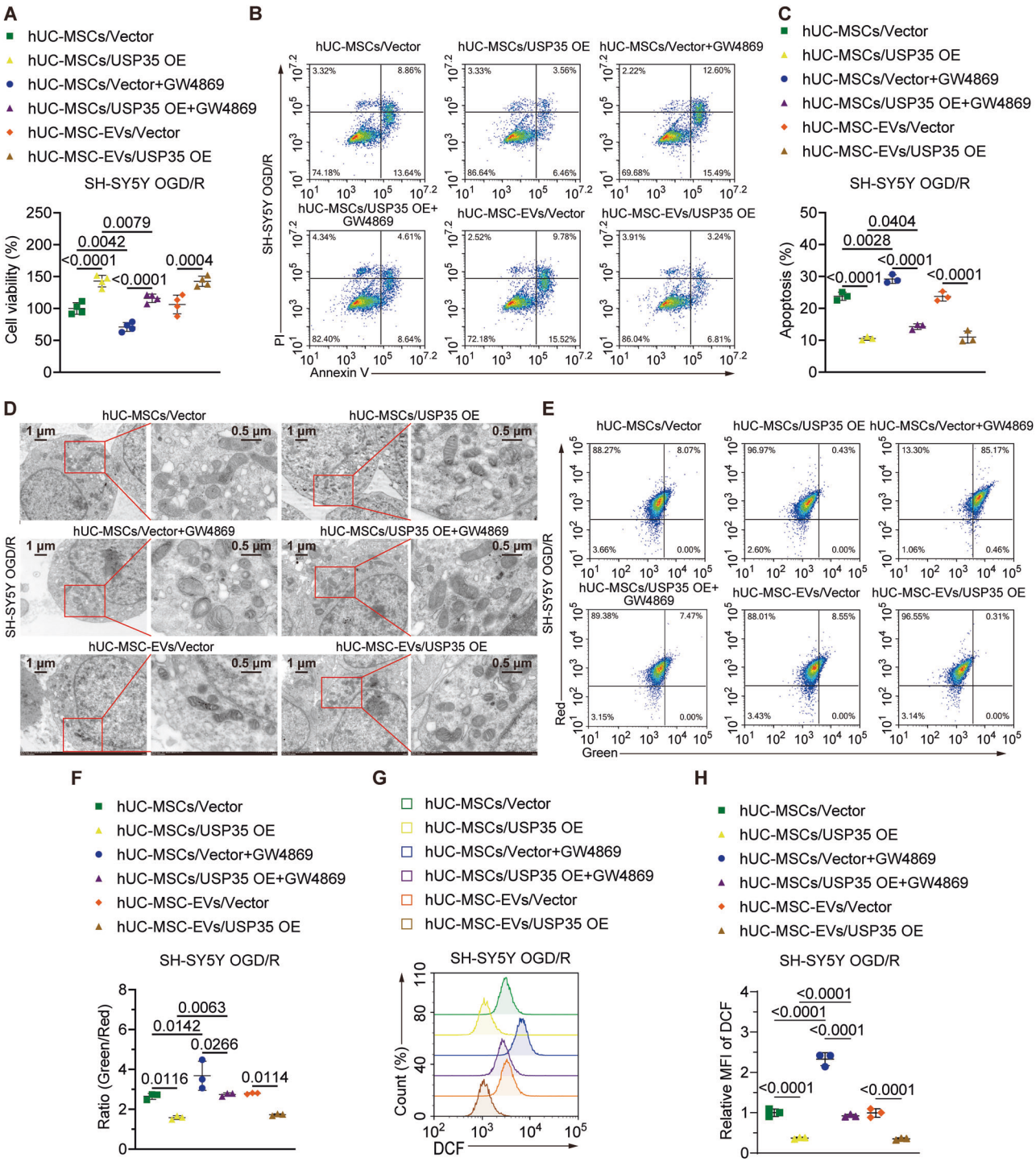

Fig. 5 | Excessive USP35 enhanced the functions of hUC-MSC and hUC-MSC-EV in improving viability, inhibiting apoptosis, reducing ROS level, and promoting autophagy in SH-SY5Y OGD/R cells. A MTT staining results demonstrated that overexpression of USP35 augmented the viability-promoting function of hUC-MSC and hUC-MSC-EV in cocultured SH-SY5Y OGD/R cells. Remarkably, excessive USP35 also enhanced the viability of SH-SY5Y OGD/R cells cocultured with GW4869-treated hUC-MSCs compared to that of SH-SY5Y OGD/R cells cocultured with hUC-MSCs. **B** Annexin V/PI staining data illustrated that USP35 overexpression reinforced the anti-apoptotic function of hUC-MSC, hUC-MSC-EV, and even GW4869-treated hUC-MSC in cocultured SH-SY5Y OGD/R cells. **C** Quantitative analysis of the Annexin V/PI staining data. **D** TEM images displayed the morphology of mitochondria in SH-SY5Y OGD/R with indicated treatments. **E** JC-1 staining data indicated that USP35 overexpression improved the effectiveness of hUC-MSC, hUC-MSC-EV, and even GW4869-treated hUC-MSC in restoring the abnormal mitochondrial membrane potential in cocultured SH-SY5Y OGD/R cells. **F** Quantification of the JC-1 staining results. **G** DCF staining results revealed that the ROS level-inhibiting function of hUC-MSC, hUC-MSC-EV, and GW4869-treated hUC-MSC was further potentiated by excessive USP35 in cocultured SH-SY5Y OGD/R cells. **H** Quantitative analysis of the DCF staining data.

Initially, we assessed the efficiency of three shRNAs targeting FUNDC1 and identified shFUNDC1-2 as the most effective in reducing FUNDC1 mRNA and protein levels (Fig. S3D and E). Subsequently, we knocked down FUNDC1 in USP35-overexpressing hUC-MSCs and examined the impact of these modified hUC-MSCs and their secreted EVs on cocultured SH-SY5Y OGD/R cells. The results demonstrated that FUNDC1 deficiency eliminated the enhanced protective effects caused by USP35 overexpression in hUC-MSCs and hUC-MSC-EVs on SH-SY5Y OGD/R cells. This was

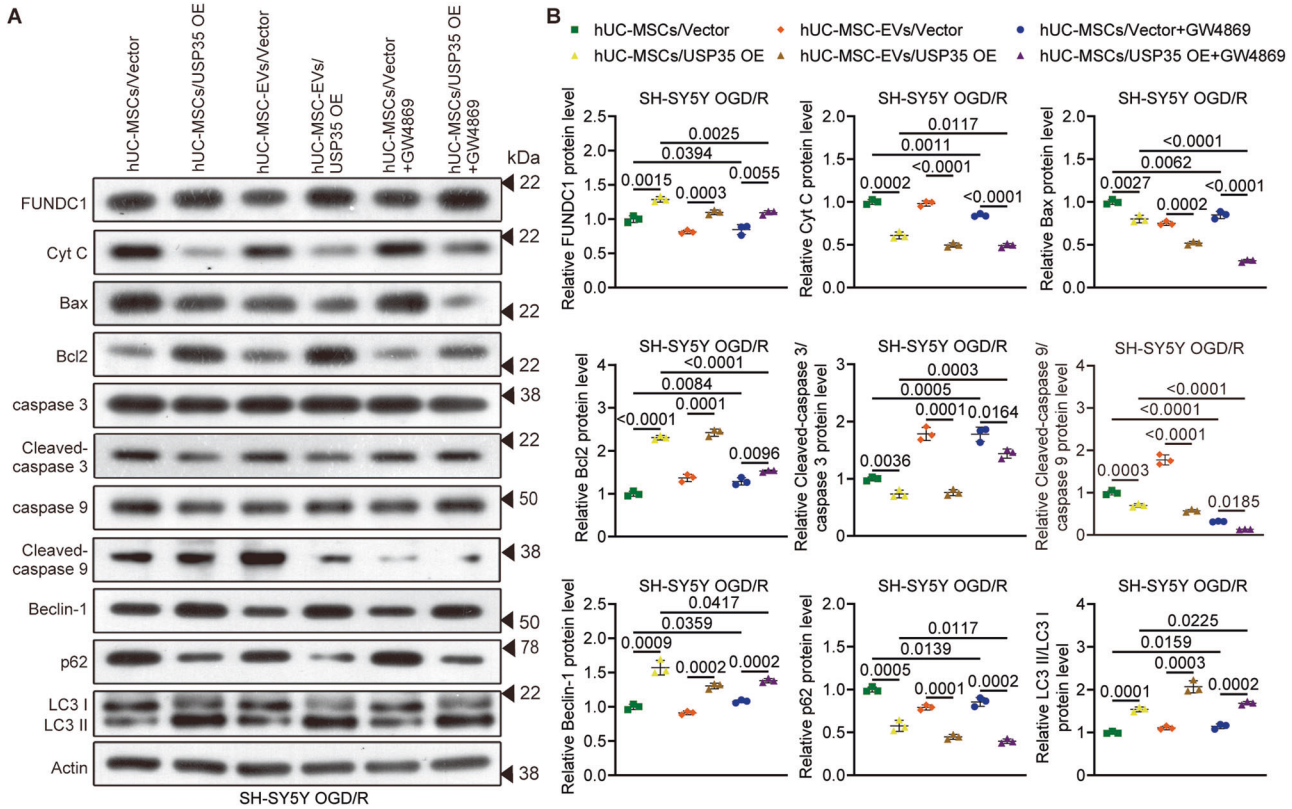

Fig. 6 | USP35 overexpression amplified the effect of hUC-MSC and hUC-MSC-EV on the expression of proteins correlated to apoptosis, ROS production, and autophagy in SH-SY5Y OGD/R cells. A Western blot results demonstrated that overexpression of USP35 augmented the effects of hUC-MSC, hUC-MSC-EV, or GW4869-treated hUC-MSC in elevating the levels of FUNDC1, Bcl2, Beclin-1, and the LC3 II/I ratio, while reducing the levels of Cyt C, Bax, cleaved-Caspase 3/9, and p62 in the cocultured SH-SY5Y OGD/R cells. **B** Quantitative analysis of the Western blot data.

manifested by decreased cell viability, heightened apoptosis, a reduced number of mitochondria, and elevated mitochondrial membrane potential and ROS levels (Fig. 7A-H). In line with these findings, Western blot data indicated that the levels of Cyt C, BAX, cleaved Caspase3/9, and p62 were elevated, whereas the levels of Bcl2, Beclin-1, and LC3 II were diminished in SH-SY5Y OGD/R cells cocultured with FUNDC1-deficient USP35-overexpressing hUC-MSCs or hUC-MSC-EVs, when compared to cells cocultured with control USP35-overexpressing hUC-MSCs or hUC-MSC-EVs (Fig. 8A and B). These findings suggest that USP35 promotes the protective effects of hUC-MSCs and hUC-MSC-EVs on SH-SY5Y OGD/R cells by stabilizing FUNDC1.

Discussion

The potential therapeutic applications of MSCs and their secreted EVs have attracted significant attention and investigation in recent years due to their promising effects on various diseases, including those associated with I/R injury[43–45]. However, the precise mechanisms underlying the therapeutic benefits of these approaches need to be thoroughly understood before their clinical application. In this study, we studied the mechanisms by which both hUC-MSCs and hUC-MSC-EVs counteract apoptosis and reduce ROS levels in a cellular model of OGD/R, which mimics CIRI. Our investigation verified the neuroprotective potential of hUC-MSCs on SH-SY5Y cells undergoing OGD/R, as evidenced by enhanced cell viability, suppressed apoptosis, decreased ROS levels, and boosted autophagy in the treated cells.

Interestingly, we found that the neuroprotective effect of hUC-MSCs was partially attenuated when EV production was blocked using GW4869, implying that EV-mediated intercellular communication plays a crucial role in mediating these beneficial effects. This observation lends further support to the idea that stem cell-derived EVs could offer an alternative therapeutic avenue for a range of conditions[46]. Importantly, GW4869 treatment did not completely abolish the beneficial effects of hUC-MSCs, which may be attributed to the incomplete blockage of EV production. Alternatively, these cells may utilize additional mechanisms, such as the secretion of soluble factors[47], to alleviate the injury induced by OGD/R in SH-SY5Y cells.

Massive neuronal cell death characterized by aberrant apoptosis and autophagy is a defining feature of CIRI[5]. It has been proposed that increased oxidative stress plays a major role in driving neuronal cell death during CIRI[48,49]. In accordance with this understanding, our study demonstrates that hUC-MSCs and their secreted EVs effectively enhance viability and reduce apoptosis in SH-SY5Y cells subjected to OGD/R. Importantly, these treatments also lead to a substantial decrease in ROS levels within the cells. This inverse relationship between cell survival and ROS levels further supports the notion that modulation of oxidative stress is pivotal for the protective effects of hUC-MSCs and hUC-MSC-EVs on SH-SY5Y OGD/R cells.

Notably, the upregulation of FUNDC1 expression, which initiates mitophagy to remove damaged mitochondria, was observed in SH-SY5Y OGD/R cells cocultured with hUC-MSCs or exposed to hUC-MSC-EVs. This observation suggests a potential mechanism by which hUC-MSCs and hUC-MSC-EVs exert their protective effects by enhancing mitophagy to reduce ROS levels in the treated cells. Nevertheless, the role of mitophagy in neurological conditions is complicated[50]. Therefore, further characterization is warranted to elucidate how enhanced mitophagy contributes to the neuroprotective effects of hUC-MSCs and their EVs.

FUNDC1, a critical regulator of mitochondrial function, is tightly controlled at both transcriptional and post-transcriptional levels[51,52]. Our study provides direct evidence that the ubiquitin-proteasome system plays a crucial role in governing the stability of the FUNDC1 protein. Our discovery of regulators that modulate the ubiquitination of FUNDC1 holds significant implications for potential therapeutic strategies targeting FUNDC1.

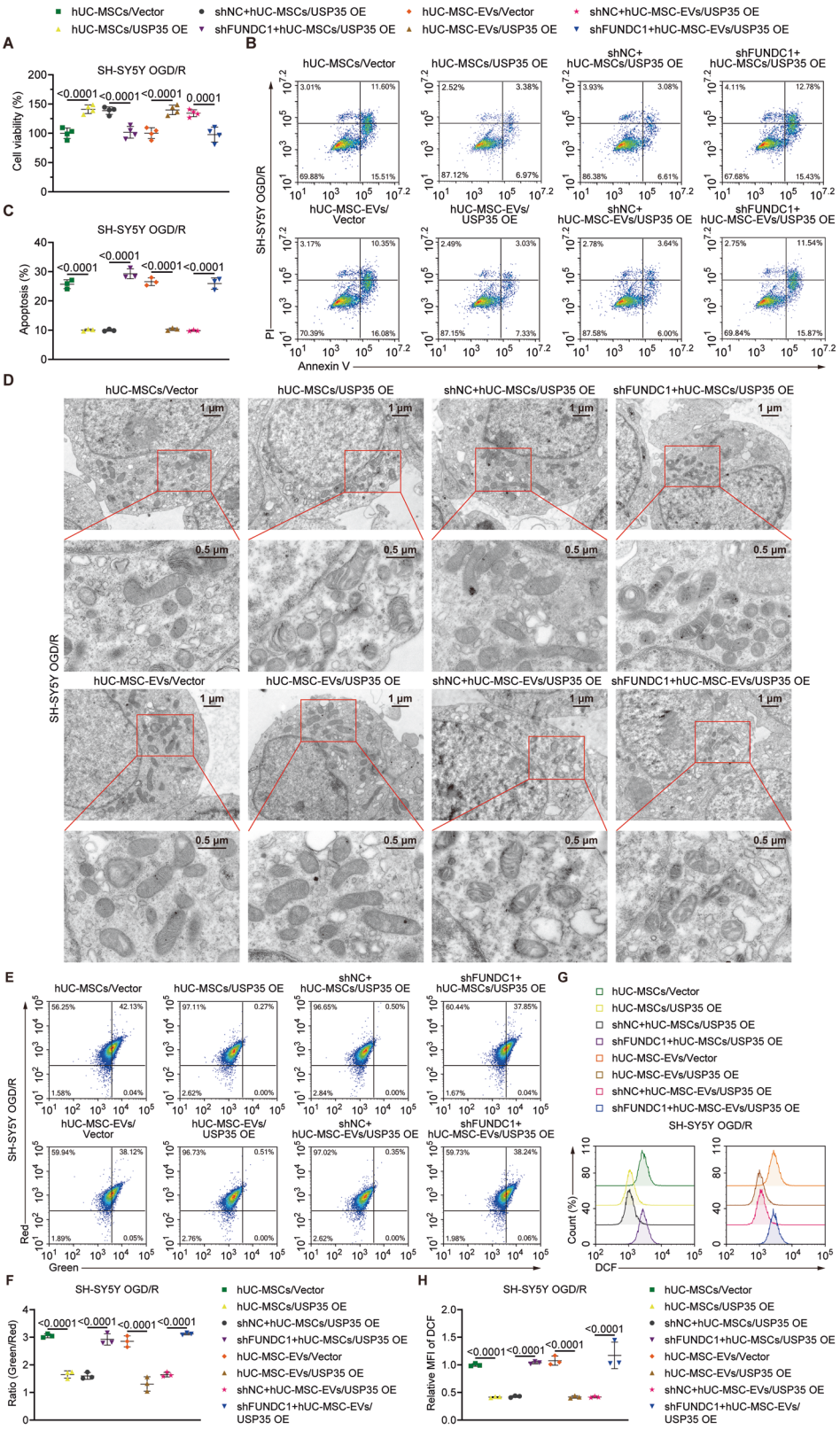

Fig. 7 | FUNDC1 deficiency abrogated the ability of excessive USP35 to enhance the effects of hUC-MSC and hUC-MSC-EV in promoting viability, reducing apoptosis, decreasing ROS levels, and inducing autophagy in SH-SY5Y OGD/R cells. **A** MTT staining results indicated that the impact of excessive USP35 on enhancing the viability-promoting function of hUC-MSC and hUC-MSC-EV in cocultured SH-SY5Y OGD/R cells was abolished by FUNDC1 deficiency. **B** Annexin V/PI staining data showed that the reinforced anti-apoptotic effect of hUC-MSC and hUC-MSC-EV on SH-SY5Y OGD/R cells through USP35 overexpression was abrogated in the context of FUNDC1 knockdown. **C** Quantification of the Annexin V/PI staining data. **D** TEM images displaying mitochondrial morphology in SH-SY5Y OGD/R cells with various treatments. **E** JC-1 staining data indicated that the enhanced capacity of hUC-MSC and hUC-MSC-EV in restoring mitochondrial membrane potential due to USP35 overexpression was no longer significant in SH-SY5Y OGD/R cells upon FUNDC1 deficiency. **F** Quantification of the JC-1 staining results. **G** DCF staining outcomes revealed that FUNDC1-deficient USP35-overexpressing hUC-MSC and hUC-MSC-EV had comparable effects to their respective controls on the ROS levels of cocultured SH-SY5Y OGD/R cells.
H Quantification of the DCF staining data.

Through a screening of 40 USPs, we identified several USPs that act as stabilizers of FUNDC1. Of these, USP35 emerged as a particularly potent regulator, as it interacts with FUNDC1 and deubiquitinates it, leading to increased FUNDC1 stability. Functionally, when USP35 was overexpressed in hUC-MSCs and hUC-MSC-EVs, both exhibited an enhanced neuroprotective effect on SH-SY5Y cells subjected to OGD/R compared to their respective control groups. However, this beneficial effect was effectively abolished upon the knockdown of FUNDC1. This highlights the critical role of the USP35-FUNDC1 axis in enhancing the neuroprotective function of both hUC-MSCs and their secreted EVs (Fig. 9). Nonetheless, it remains to be investigated whether other USPs might also contribute to the stabilization of FUNDC1 in hUC-MSCs and participate in the mediation of their

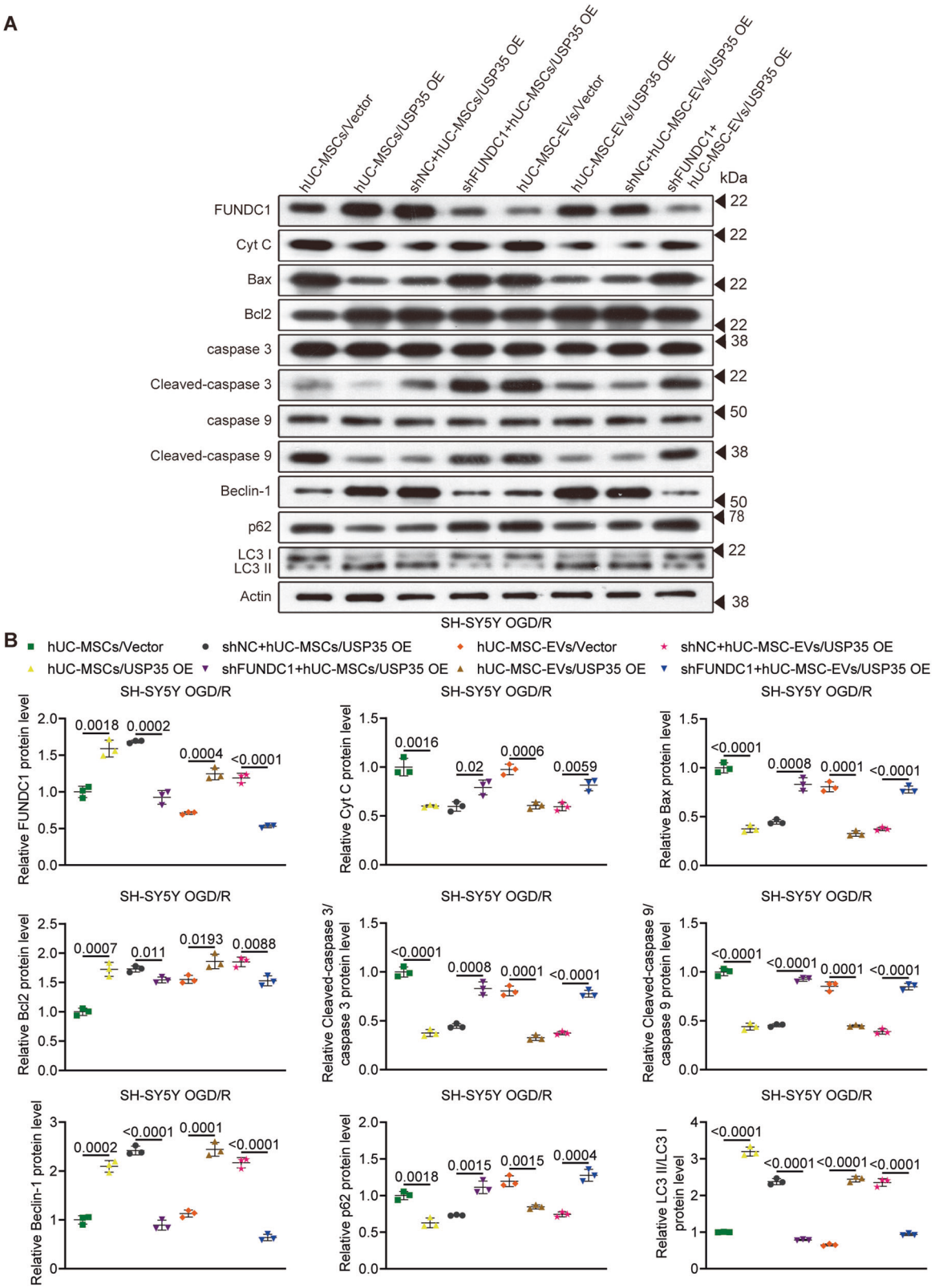

Fig. 8 | FUNDC1 was required for USP35 to reinforce the impact of hUC-MSC and hUC-MSC-EV on the expression of proteins associated with apoptosis, ROS production, and autophagy in SH-SY5Y OGD/R cells. A Western blot results revealed that FUNDC1 deficiency eliminated the effect of excessive USP35 in strengthening the regulation by hUC-MSC and hUC-MSC-EV to increase the levels of FUNDC1, Bcl2, Beclin-1, and LC3 II/I ratio, as well as to decrease the levels of Cyt C, Bax, cleaved-Caspase 3/9, and p62 in the cocultured SH-SY5Y OGD/R cells. **B** Quantification of the Western blot data.

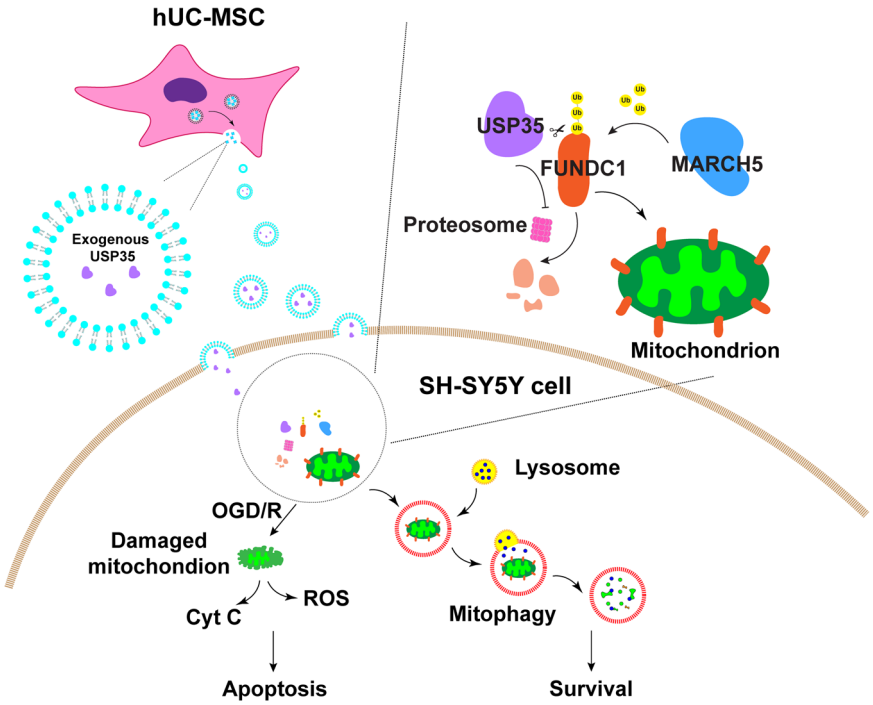

Fig. 9 | Schematic presentation of the conclusions of our study.

neuroprotective effects. Further exploration is necessary to elucidate the broader regulatory network underlying FUNDC1 stabilization in hUC-MSCs and its involvement in their therapeutic potential.

USP35 has been implicated in the progression of various cancer types, such as ovarian, prostate, lung, and melanoma[53–57], where it exerts its effects through modulation of substrates like STING, ribosome binding proteins, aurora kinase, and NRF2[55,57–59]. Our discovery that USP35 also plays a role in regulating the stability of FUNDC1 adds another layer of complexity to the repertoire of targets under the control of USP35. Investigating whether other substrates of USP35 contribute to its effects on enhancing the neuroprotective functions of hUC-MSCs and hUC-MSC-EVs could provide valuable insights into the multifaceted mechanisms underlying these effects.

The catalytic domain of USPs is crucial for their function. Overexpressing USP35 with a non-functional catalytic domain nullifies its ability to enhance the protective effects of hUC-MSC-EVs on cocultured SH-SY5Y OGD/R cells. However, the specific domain of FUNDC1 that interacts with USP35 has yet to be identified. Additionally, the overexpression of mutant USP35 likely interferes with the function of endogenous USP35. Since USP35 deficiency has little impact on the protective role of hUC-MSC-EVs in SH-SY5Y OGD/R cells, it suggests that hUC-MSCs and their EVs utilize multiple mechanisms, such as the delivery or regulation of other USPs, to perform their protective functions. Therefore, endogenous USP35 is not essential for the neuroprotective effects of hUC-MSCs and their EVs in this context.

Notably, our study only revealed that overdosed exogenous USP35 encapsulated in hUC-MSC-EVs inhibits apoptosis and mitochondrial damage by stabilizing FUNDC1 in OGD/R-induced SH-SY5Y cells at the cellular level. The lack of animal experiments to verify these results is another limitation of this study.

In conclusion, our study has substantiated that hUC-MSCs and their secreted EVs possess the ability to inhibit apoptosis and reduce ROS levels within an in vitro CIRI model. This neuroprotective function is likely attributed to elevated levels of FUNDC1 protein. Moreover, the augmentation of hUC-MSC and hUC-MSC-EV function can be strengthened through the overexpression of USP35, which leads to the stabilization of FUNDC1. These findings not only expand our understanding of the mechanisms underlying the beneficial effects of hUC-MSC and hUC-MSC-EV in mitigating CIRI and the regulation of FUNDC1 metabolism but also highlight the USP35-FUNDC1 axis as a therapeutical target for the treatment of symptoms arising from CIRI.

Methods

Cell lines and cell culture

SH-SY5Y neuroblastoma cells, HEK293T cells, and hUC-MSCs were procured from Immocell Biotechnology (Xiamen, China). These cells were cultured in DMEM supplemented with 10% FBS (Thermo Fisher Scientific) and 1% penicillin/streptomycin (Thermo Fisher Scientific) within a humidified incubator set at 37°C with 5% CO_2. Before use, all cells underwent testing for Mycoplasma contamination twice a week using the Plasmo Test (InvivoGen). The cells were passaged 2 to 5 times for the experiments after recovery from cryopreservation in liquid nitrogen. For specific experiments, the culture media were supplemented with 30 μM Cycloheximide (CHX), 10 or 20 μM MG132, and/or 5 μM of GW4869 (MedChemExpress) as indicated.

Plasmid construction

For the purpose of screening potential USP family members that might regulate FUNDC1, the coding sequences of the specified USPs, along with the HA-tag coding sequence, were individually incorporated into the pcDNA3.3 vector backbone. Additionally, G4S-FUNDC1 was cloned into the pmirGLO vector to facilitate the luciferase assay. The 40 USPs examined in this study were USP1, 2, 3, 4, 5, 6, 7, 8, 10, 11, 13, 14, 15, 18, 19, 20, 21, 22, 25, 26, 27X, 29, 30, 32, 33, 35, 36, 38, 39, 40, 44, 45, 46, 48, 49, L1, 51, 52, 53, 54. These plasmids were obtained from Anti-hela Biological Technology (Xiamen, China).

To assess the ubiquitination of FUNDC1, either Flag-tagged FUNDC1 or HA-tagged wild-type (WT) or catalytic domain-deficient (mut) USP35 was cloned into the pcDNA3.3 vector, coupled with a puromycin expression cassette for facilitating overexpression screening. Furthermore, His-tagged ubiquitin was also introduced into the pcDNA3.3 vector.

To knock down USP35 or FUNDC1, specific shRNAs targeting either USP35 or FUNDC1 were cloned into the pLKO.1 lentiviral backbone. The production of lentivirus was conducted by Anti-hela Biological Technology (Xiamen, China), utilizing the four-plasmid system[60]. This process was performed in HEK293T cells.

The following primer sequences were used: pcDNA3.3-HA-USP35-F: 5′-TAGAGAATTCGGATCCATGGACAAGATCTTGGAGGCGGTG-3′, pcDNA3.3-HA-USP35-R: 5′-GCTTCCATGGCTCGAGTTAGAAGACCAGTCTGTGGAAGTC-3′; pcDNA3.3-HA-USP35-mut-F: 5'-GGCAACACAGCCTATGTCAACAGCATCCTTC-3', pcDNA3.3-HA-USP35-mut-R: 5'- TTGACATAGGCTGTGTTGCCCAGGTTGATG-3'; pcDNA3.3-FUNDC1-F: 5′-TAGAGAATTCGGATCCATGGCGACCCGGAACCCCCC-3′, FUNDC1-flag-R: 5′-TGTCGTCATCGTCTTTGTAGTCAGATGCAAGTCCGAGCAAAAAGCCTCCC-3′, pcDNA3.3-flag-R: 5′-GCTTCCATGGCTCGAGTCACTTGTCGTCATCGTCTTTGTAG-3′; shUSP35-1-F: 5′-CCGGCGGAGAGTGGTCACTACTACTCTCGAGAGTAGTAGTGACCACTCTCCGTTTTT-3′, shUSP35-1-R: 5′- AATTAAAAACGGAGAGTGGTCACTACTACTCTCGAGAGTAGTAGTGACCACTCTCCG-3′; shUSP35-2-F: 5′-CCGGCCTTGTCTGTGCTCAAGTACACTCGAGTGTACTTGAGCACAGACAAGGTTTTT-3′, shUSP35-2-R: 5′-AATTAAAAACCTTGTCTGTGCTCAAGTACACTCGAGTGTACTTGAGCACAGACAAGG-3′; shFUNDC1-1-F: 5′-CCGGCTTCAGATTGCTAGTCATAGTCTCGAGACTATGACTAGCAATCTGAAGTTTTT-3′, shFUNDC1-1-R: 5′-AATTAAAAACTTCAGATTGCTAGTCATAGTCTCGAGACTATGACTAGCAATCTGAAG-3′; shFUNDC1-2-F: 5′-CCGGCCAAGACTATGAAAGTGATGACTCGAGTCATCACTTTCATAGTCTTGGTTTTT-3′, shFUNDC1-2-R: 5′-AATTAAAAACCAAGACTATGAAAGTGATGACTCGAGTCATCACTTTCATAGTCTTGG-3′; shFUNDC1-3-F: 5′-CCGGGTAGCTACCCAGATTGTAATGCTCGAGCATTACAATCTGGGTAGCTACTTTTT-3′, shFUNDC1-3-R: 5′-AATTAAAAAGTAGCTACCCAGATTGTAATGCTCGAGCATTACAATCTGGGTAGCTAC-3′.

Cell transfection

Lipofectamine 3000 (Invitrogen) was employed for non-viral plasmid transfections, following the guidelines provided by the manufacturer. The procedure involved seeding cells onto 24-well plates until they reached approximately 70% confluence. Subsequently, plasmids were combined with Opti-MEM (Thermo Fisher Scientific), and the mixture was then diluted with Lipofectamine and P3000 reagent. This combination was thoroughly mixed before being introduced into the cell culture. After that, cells were allowed to incubate for 48 hours before being harvested for further analysis in subsequent experiments.

For lentivirus infection, cells were cultivated until they reached around 70% confluence. Virus stocks were suitably diluted in Opti-MEM and subsequently introduced into the cell culture based on a previously determined optimized MOI (Multiplicity of Infection) specific to either hUC-MSCs (MOI = 50) or SH-SY5Y cells (MOI = 20). Following this, the media containing the virus was replenished 24 hours after infection. 48 hours after initial infection, puromycin was introduced to the media at a final concentration of 3 μg/ml. This selective agent was employed to screen and retain cells that exhibited resistance to puromycin. Cells that successfully survived the puromycin selection process were collected for subsequent analyses 80 hours after the initial transfection.

Flow cytometry analysis

For the analysis of each cell surface marker, 1×10^6 isolated hUC-MSCs were collected and suspended in 50 μL of FACS buffer. Dye-conjugated antibodies were appropriately diluted in 50 μL of FACS buffer according to the recommended dilution ratios provided by the manufacturers. The antibody solutions were thoroughly mixed with the cell suspension and allowed to incubate on ice for 30 minutes in a dark environment. Following this incubation, the samples were subjected to two rounds of washing with FACS buffer. Subsequently, the samples were subjected to flow cytometry analysis using a NovoCyte FACS cytometer (Agilent).

Flowjo software (BD Bioscience) was utilized to calculate the mean fluorescent intensity (MFI) from the FACS data. The following antibodies from BioLegend were employed for the flow cytometry analysis: CD14 (Cat#: 325603, 1:100), CD19 (Cat#: 302205, 1:100), CD34 (Cat#: 343503, 1:100), CD45 (Cat#: 304005, 1:100), HLA-DR (Cat#: 980402, 1:100), CD29 (Cat#: 303004, 1:100), CD44 (Cat#: 397517, 1:100), CD73 (Cat#: 344016, 1:100), CD90 (Cat#: 328107, 1:100), CD105 (Cat#: 323204, 1:100).

Induced differentiation of hUC-MSC

To evaluate the pluripotency of the isolated hUC-MSCs, the cells were induced to undergo osteogenic, adipogenic, or chondrogenic differentiation using the following STEMPRO® kits from Thermo Fisher Scientific: Osteogenesis Differentiation Kit (A1007201), Adipogenesis Differentiation Kit (A1007001), and Chondrogenesis Differentiation Kit (A1007101), respectively, according to the manufacturer's protocols. Briefly, hUC-MSC cells were seeded onto gelatin-coated 6-well plates and allowed to reach approximately 70% confluence. At this point, induction media, prewarmed to 37 °C, were introduced after discarding the existing media. The induction period lasted for 2 weeks, during which the induction media were replaced every 3 days. At the end of the induction period, the presence of differentiated cells was determined using specific staining methods: alizarin red for osteocytes, oil red O for adipocytes, and alcian blue for chondrocytes.

For alizarin red staining: Fixed cells were treated with 60% isopropanol for 1 minute at RT, followed by washing with PBS and staining with 10% alizarin red solution for 15 minutes at RT. The cells were then rinsed with PBS. For alcian blue staining: Fixed cells were incubated with a 1% alcian blue/0.1 N HCl solution for 30 minutes, followed by washing with 0.1 N HCl and immersion in distilled water. For oil red O staining: Fixed cells were stained with a 0.5% oil red O/isopropanol solution for 5 minutes at 37 °C in the dark.

EV isolation and purification

1×10^7 hUC-MSCs were seeded into a T175 (175 CM^2) culture flask (Corning) and cultured with DMEM medium containing 10% EV-free FBS for 48 hours. The culture media were collected and underwent a series of centrifugation steps to isolate EVs. First, the culture media were centrifuged sequentially at 300 g, 2000 g, and 12,000 g to collect the supernatant. Following this, the supernatant, containing the EVs, was subjected to ultracentrifugation at 100,000 g for 60 minutes at 4 °C. Subsequently, the resulting supernatant was discarded, and the pellet was resuspended using PBS. After the initial resuspension, another round of ultracentrifugation and resuspension of the pellet were carried out. Following the third round of ultracentrifugation, the final pellet was resuspended in 100 μL of ice-cold PBS. This resuspended pellet was then divided into smaller aliquots for the purpose of further characterization and subsequent experimental procedures. To validate the efficacy of GW4869 treatment, the culture medium from GW4869-treated cells was collected and subjected to EV isolation and purification using identical procedures as those for untreated cells. The same volume of resuspended EV solutions was then loaded for Western blot analysis.

TEM and NTA

TEM and NTA were performed by Pinuofei Biological Technology (Wuhan, China). For the TEM sample preparation, the cell culture media were discarded, and the cells were treated with 2.5% glutaraldehyde for fixation. Subsequently, the cells were subjected to digestion, pelleted, resuspended, and then fixed once again using 2.5% glutaraldehyde. This final fixation step lasted for 2 hours at room temperature (RT).

Establishment of cellular IR model by OGD and reperfusion

SH-SY5Y cells without coculture with hUC-MSCs or hUC-MSC-EVs were designated as "Mock". For SH-SY5Y in the hUC-MSC group, SH-SY5Y cells were seeded into 6-well plates at a density of 8×10^4 per well. Concurrently, hUC-MSC cells were inoculated into Transwell (Corning) at a density of 8×10^4 per well and then cocultured with SH-SY5Y cells for 48 hours. For SH-SY5Y cells in the hUC-MSC-EV group, the SH-SY5Y cells were seeded into 6-well plates at a density of 8×10^4 per well and cultured with 60 μg hUC-MSC-EV for 48 hours. To initiate OGD/R, the SH-SY5Y cells in all groups were cultured in glucose-free DMEM (Thermo Fisher Scientific) and transferred to a hypoxic humidified incubator (StemCell Technologies, Canada) operating at 37°C. This specialized incubator was supplied with an

environment containing 1% O_2 and 5% CO_2, as previously outlined[34–36]. The cells were subjected to this hypoxic condition for a duration of 4 hours. Subsequent to the OGD treatment, the culture medium was switched back to normal DMEM media (Thermo Fisher Scientific) containing 10% FBS. The cells were maintained in a humidified incubator set at 37°C and supplied with 5% CO_2, for a specified period (3, 6, 12, or 24 hours).

Annexin V-FITC/PI analysis

To assess apoptosis, the Annexin V-FITC/PI apoptosis detection kit (Vazyme) was employed following the provided instructions. In brief, 1×10^6 SH-SY5Y cells were collected and suspended in 100 μL of binding buffer. Subsequently, a mixture of 5 μL of Annexin-V FITC and 5 μL of PI solutions was combined with the cell suspension. This mixture was then incubated at RT for 10 minutes while keeping it in the dark. Following the incubation, 400 μL of binding buffer was added to the cell suspension subjected to flow cytometry analysis. For compensation adjustment, single staining with either Annexin-V FITC or PI was also included. The flow cytometry results were analyzed using Flowjo (BD Bioscience). All flow cytometry experiments were performed in triplicate.

JC-1 mitochondrial membrane potential assay

To evaluate mitochondrial membrane potential, the JC-1 assay kit (Beyotime Biotechnology) was employed in accordance with the manufacturer's instructions. In brief, 5×10^5 SH-SY5Y cells were suspended in 500 μL of culture media and then mixed with 500 μL of JC-1 working solution. This mixture was incubated for 20 minutes at 37 °C. Subsequently, the cells were pelleted, washed, and then resuspended in JC-1 wash buffer. The cells were then subjected to flow cytometry analysis using the FITC or PE channel for detecting monomers or aggregates of JC-1, respectively. The data were further analyzed using Flowjo. This analysis involved gating and quantifying the proportion of FITC+ and/or PE+ cells. Additionally, the ratio of the FITC + /PE+ proportion, also known as the Green/Red ratio, was calculated for comparison among different experimental groups.

CFSE staining

CellTrace™ CFSE proliferation kit (Invitrogen) was utilized to label hUC-MSC-EVs following the manufacturer's protocol. To outline the process, CFSE was diluted at a ratio of 1:1000 in the culture medium of hUC-MSCs. The cell culture was then maintained for a duration of 2 hours in a light-protected environment. Subsequently, the medium containing CFSE was removed, and the cells were subjected to washing steps before being placed in prewarmed fresh media. This process aimed to generate CFSE-labeled EVs. Afterward, the conditioned media, enriched with CFSE-labeled EVs, was utilized for incubation with SH-SY5Y cells cultured on microslides. After the incubation, the cells were fixed and subsequently stained with DAPI to visualize the cellular nuclei. Fluorescence imaging was performed using a Zeiss LSM 710 confocal microscope.

ROS detection

The DCFDA/H2DCFDA cellular ROS assay kit (ab113851, Abcam) was utilized for ROS detection. Briefly, SH-SY5Y cells were stained with DCFDA at 37 °C for 30 minutes in the dark. Afterward, the cells were washed, resuspended, and seeded into a microplate at 100,000 cells per well. The plate was subsequently measured by flow cytometry, and the MFI of each well was documented, normalized to mock, and analyzed to determine the ROS level of each group.

MTT assay

MTT (Beyotime Biotechnology) was used to measure cell viability. In brief, SH-SY5Y cells were inoculated into 96-well plates at a density of ~2000 cells/well. Subsequently, 10 μL of 5 mg/ml MTT solution was added to each well, and the plates were incubated at 37°C for 4 hours. After the supernatant in the wells was carefully aspirated, 150 μl of DMSO was added to each well, and the cell culture plate was shaken for 10 min to dissolve the crystals. Finally, the OD_{570} value of each well was measured using a microplate reader. Biological triplicates were set and analyzed for each group and each experiment was repeated at least three times. The results from other groups of cells were normalized to those from the "Mock" group.

RNA extraction and qPCR

Total RNA was extracted using Trizol reagent (Invitrogen) and was subjected to reverse transcription by PrimeScript RT Master Mix (Takara). qPCR experiments were performed with a CFX96 machine (BioRad) using EvaGreen 2x qRT-PCR Mastermix (Applied Biological Materials). The expression of target genes was calculated using the $2^{-\Delta\Delta Ct}$ method. The primers used for qPCR are listed as follows: USP35-F: 5′-TCAGATA TGGAAGTAAGACCTAAG-3′, USP35-R: 5′-TCGGCTGCTTCAAGTT AA-3′, FUNDC1-F: 5′-AGACACCAGTGGTGGAATCGAG-3′, FUND C1-R: 5′-TCTGGAACAGAAATCCTGCACAC-3′, 18 s rRNA-F: 5′-CGA CGACCCATTCGAACGTCT-3′, 18 s rRNA-R: 5′-CTCTCCGGAATC-GAA CCCTGA-3′.

IP and Western blot

SH-SY5Y cells were cultured in 6-well plates, and proteins were extracted using protease inhibitor-containing RIPA lysis buffer (Beyotime Biotechnology, 800 μl per well) and quantified using a BCA kit. 50 μl of each sample was mixed with 5X loading buffer and denatured. 5 μl of the resulting mixture was used as total cell lysate (TCL). The remaining 750 μl sample that contains approximately 50 μg total protein was subjected to IP assay, and 2 μg antibody against Flag-tag (Proteintech, Cat#:66008-4-Ig) or HA-tag (Proteintech, Cat#: 66006-2-Ig) was pre-incubated with Dynabeads™ (Invitrogen) in the Ab binding & washing buffer included in the IP kit (Invitrogen) for 15 minutes. Then the antibody-conjugated beads were washed and incubated with the protein samples with gentle shaking. Finally, the beads were pelleted and 20 μL elution buffer was applied to elute the binding proteins, and 5 μl of eluted proteins was used for Western blot analysis.

For Western Blot, the protein samples were mixed with loading buffer and denatured at 95 °C for 5 minutes. The samples were then subjected to SDS-PAGE separation (15 μg/well) and were transferred to PVDF membranes, which were blocked in the 5% nonfat powdered milk solution (Beyotime Biotechnology). Afterwards, the membranes were incubated with the corresponding primary antibodies overnight at 4°C. After washing with TBST solution, the membranes were incubated with secondary antibodies for 2 hours at RT. Finally, the membranes were washed with TBST and incubated with ECL reagent. The signals were visualized and imaged using the ChemiDoc imaging system (BioRad). The band intensity was quantified by ImageJ software (NIH) and normalized to the housekeeping gene that served as internal control. The experiments were repeated three times for statistical analysis. β-actin was used as the loading control. The antibodies for Western Blot and their dilution are listed as follows: USP35 (Proteintech, Cat#: 24559-1-AP, 1:1000), FUNDC1 (Proteintech, Cat#: 28519-1-AP, 1:2000), Cyt C (Proteintech, Cat#: 10993-1-AP, 1:1000), BAX (Proteintech, Cat#: 50599-2-Ig, 1:1000), BCL2 (Proteintech, Cat#: 12789-1-AP, 1:2000), total and cleaved Caspase 3 (Proteintech, Cat#: 19677-1-AP, 1:1000), total and cleaved Caspase 9 (Proteintech, Cat#: 10380-1-AP, 1:1000), Beclin-1 (Proteintech, Cat#: 11306-1-AP, 1:1000), p62 (Proteintech, Cat#: 18420-1-AP, 1:5000), LC3 I/II (Proteintech, Cat#: 14600-1-AP, 1:1000), Flag (Proteintech, Cat#: 20543-1-AP, 1:20000), HA (Proteintech, Cat#: 51064-2-AP, 1:5000), His (Proteintech, Cat#: 10001-0-AP, 1:1000), β-actin (Proteintech, Cat#: 20536-1-AP, 1:1000), Luciferase (Proteintech, Cat#: 27986-1-AP, 1:1000), CD9 (Proteintech, Cat#: 20597-1-AP, 1:1000), CD81 (Proteintech, Cat#: 27855-1-AP, 1:1000), CD63 (Proteintech, Cat#: 25682-1-AP, 1:1000), horseradish peroxidase-conjugated goat anti-rabbit IgG (Proteintech, Cat#: SA00001-2, 1:2000). In experiments using a protein ladder without chemiluminescence conjugation, the position of the protein ladder was marked by manually aligning the exposed films with the PVDF membranes.

Luciferase assay

After 48 hours of transfection, the cells were harvested and lysed. The luciferase activity was determined using the Dual-Luciferase Reporter Assay

System (Promega) on a microplate reader. Firefly luciferase activity was normalized to Renilla luciferase activity in each sample.

Statistics and reproducibility

Unpaired two-tailed Student's *t*-test and one-way ANOVA test were used to calculate the difference between two groups of data and among multiple groups of data, respectively. Data were presented as mean ± SD. Graphic visualization and data analyses were carried out by Prism (v8, GraphPad). All experiments were independently repeated at least three times. Additionally, for luciferase, MTT, and qPCR assays, each sample was tested in triplicate.

Reporting summary

Further information on research design is available in the Nature Portfolio Reporting Summary linked to this article.

Data availability

The authors declare that the main data supporting the conclusions of the current study is available within the manuscript and its Supplementary files. The uncropped Western blot results are shown as Figs. S5-S16. The numerical source data for graphs and charts is shown in Supplementary Data 1. This study includes no data deposited in external repositories. All other data are available from the corresponding author on reasonable request.

Received: 21 November 2023; Accepted: 7 October 2024;
Published online: 15 October 2024

References

1. Powers, W. J. Acute Ischemic Stroke. *N. Engl. J. Med*. **383**, 252–260 (2020).
2. Feske, S. K. Ischemic Stroke. *Am. J. Med*. **134**, 1457–1464 (2021).
3. Kalogeris, T., Baines, C. P., Krenz, M. & Korthuis, R. J. Cell biology of ischemia/reperfusion injury. *Int Rev. Cell Mol. Biol.* **298**, 229–317 (2012).
4. Datta, A. et al. Cell Death Pathways in Ischemic Stroke and Targeted Pharmacotherapy. *Transl. Stroke Res*. **11**, 1185–1202 (2020).
5. Zhang, Q., Jia, M., Wang, Y., Wang, Q. & Wu, J. Cell Death Mechanisms in Cerebral Ischemia-Reperfusion Injury. *Neurochem Res*. **47**, 3525–3542 (2022).
6. Wu, L. et al. Curcumin exerts protective effects against hypoxia-reoxygenation injury via the enhancement of apurinic/apyrimidinic endonuclease 1 in SH-SY5Y cells: Involvement of the PI3K/AKT pathway. *Int J. Mol. Med*. **45**, 993–1004 (2020).
7. Mokhtari Sangdehi, S. R., Hajizadeh Moghaddam, A. & Ranjbar, M. Anti-apoptotic effect of silymarin-loaded chitosan nanoparticles on hippocampal caspase-3 and Bcl-2 expression following cerebral ischemia/reperfusion injury. *Int J. Neurosci.* **132**, 1102–1109 (2022).
8. Shi, Y. et al. Isoquercetin Improves Inflammatory Response in Rats Following Ischemic Stroke. *Front Neurosci.* **15**, 555543 (2021).
9. Wajant, H., Pfizenmaier, K. & Scheurich, P. Tumor necrosis factor signaling. *Cell Death Differ.* **10**, 45–65 (2003).
10. Huang, Y. G. et al. Autophagy: novel insights into therapeutic target of electroacupuncture against cerebral ischemia/ reperfusion injury. *Neural Regen. Res*. **14**, 954–961 (2019).
11. Zhang, X. et al. Cerebral ischemia-reperfusion-induced autophagy protects against neuronal injury by mitochondrial clearance. *Autophagy* **9**, 1321–1333 (2013).
12. Brown, C. et al. Mesenchymal stem cells: Cell therapy and regeneration potential. *J. Tissue Eng. Regen. Med*. **13**, 1738–1755 (2019).
13. Ding, D. C., Chang, Y. H., Shyu, W. C. & Lin, S. Z. Human umbilical cord mesenchymal stem cells: a new era for stem cell therapy. *Cell Transpl.* **24**, 339–347 (2015).
14. Drela, K., Stanaszek, L., Nowakowski, A., Kuczynska, Z. & Lukomska, B. Experimental Strategies of Mesenchymal Stem Cell Propagation: Adverse Events and Potential Risk of Functional Changes. *Stem Cells Int* **2019**, 7012692 (2019).
15. Gatti, S. et al. Microvesicles derived from human adult mesenchymal stem cells protect against ischaemia-reperfusion-induced acute and chronic kidney injury. *Nephrol. Dial. Transpl.* **26**, 1474–1483 (2011).
16. Zhou, Y. et al. Exosomes released by human umbilical cord mesenchymal stem cells protect against cisplatin-induced renal oxidative stress and apoptosis in vivo and in vitro. *Stem Cell Res. Ther.* **4**, 34 (2013).
17. Mao, F. et al. Exosomes Derived from Human Umbilical Cord Mesenchymal Stem Cells Relieve Inflammatory Bowel Disease in Mice. *Biomed. Res. Int* **2017**, 5356760 (2017).
18. Wei, Z. et al. Human umbilical cord mesenchymal stem cells derived exosome shuttling mir-129-5p attenuates inflammatory bowel disease by inhibiting ferroptosis. *J. Nanobiotechnol.* **21**, 188 (2023).
19. Song, Y. et al. Human umbilical cord blood-derived MSCs exosome attenuate myocardial injury by inhibiting ferroptosis in acute myocardial infarction mice. *Cell Biol. Toxicol.* **37**, 51–64 (2021).
20. Zhao, Y. et al. Exosomes Derived from Human Umbilical Cord Mesenchymal Stem Cells Relieve Acute Myocardial Ischemic Injury. *Stem Cells Int* **2015**, 761643 (2015).
21. Hu, Z. et al. Human Umbilical Cord Mesenchymal Stem Cell-Derived Exosomes Attenuate Oxygen-Glucose Deprivation/Reperfusion-Induced Microglial Pyroptosis by Promoting FOXO3a-Dependent Mitophagy. *Oxid. Med. Cell Longev.* **2021**, 6219715 (2021).
22. Wan, Y. et al. Human umbilical cord mesenchymal stem cell exosomes alleviate acute kidney injury by inhibiting pyroptosis in rats and NRK-52E cells. *Ren. Fail* **45**, 2221138 (2023).
23. Hershko, A. & Ciechanover, A. The ubiquitin system. *Annu Rev. Biochem* **67**, 425–479 (1998).
24. Clague, M. J. et al. Deubiquitylases from genes to organism. *Physiol. Rev.* **93**, 1289–1315 (2013).
25. Komander, D., Clague, M. J. & Urbe, S. Breaking the chains: structure and function of the deubiquitinases. *Nat. Rev. Mol. Cell Biol.* **10**, 550–563 (2009).
26. Mevissen, T. E. T. & Komander, D. Mechanisms of Deubiquitinase Specificity and Regulation. *Annu Rev. Biochem* **86**, 159–192 (2017).
27. Faesen, A. C. et al. The differential modulation of USP activity by internal regulatory domains, interactors and eight ubiquitin chain types. *Chem. Biol.* **18**, 1550–1561 (2011).
28. Liu, L. et al. Mitochondrial outer-membrane protein FUNDC1 mediates hypoxia-induced mitophagy in mammalian cells. *Nat. Cell Biol.* **14**, 177–185 (2012).
29. Cai, Y. et al. FUNDC1-dependent mitophagy induced by tPA protects neurons against cerebral ischemia-reperfusion injury. *Redox Biol.* **38**, 101792 (2021).
30. Chen, Z. et al. Mitochondrial E3 ligase MARCH5 regulates FUNDC1 to fine-tune hypoxic mitophagy. *EMBO Rep.* **18**, 495–509 (2017).
31. Lv, F. J., Tuan, R. S., Cheung, K. M. & Leung, V. Y. Concise review: the surface markers and identity of human mesenchymal stem cells. *Stem Cells* **32**, 1408–1419 (2014).
32. Uder, C., Bruckner, S., Winkler, S., Tautenhahn, H. M. & Christ, B. Mammalian MSC from selected species: Features and applications. *Cytom. A* **93**, 32–49 (2018).
33. Kowal, E. J. K., Ter-Ovanesyan, D., Regev, A. & Church, G. M. Extracellular Vesicle Isolation and Analysis by Western Blotting. *Methods Mol. Biol.* **1660**, 143–152 (2017).
34. Marutani, E. et al. A novel hydrogen sulfide-releasing N-methyl-D-aspartate receptor antagonist prevents ischemic neuronal death. *J. Biol. Chem.* **287**, 32124–32135 (2012).
35. Xiao, B. et al. Endothelial cell-derived exosomes protect SH-SY5Y nerve cells against ischemia/reperfusion injury. *Int J. Mol. Med.* **40**, 1201–1209 (2017).
36. Zeng, X. et al. Activated Drp1 regulates p62-mediated autophagic flux and aggravates inflammation in cerebral ischemia-reperfusion via the ROS-RIP1/RIP3-exosome axis. *Mil. Med Res.* **9**, 25 (2022).

37. Kim, J. H., Lee, C. H. & Baek, M. C. Dissecting exosome inhibitors: therapeutic insights into small-molecule chemicals against cancer. *Exp. Mol. Med.* **54**, 1833–1843 (2022).
38. Chang, K. C. et al. The interplay of autophagy and oxidative stress in the pathogenesis and therapy of retinal degenerative diseases. *Cell Biosci.* **12**, 1 (2022).
39. Filomeni, G., De Zio, D. & Cecconi, F. Oxidative stress and autophagy: the clash between damage and metabolic needs. *Cell Death Differ.* **22**, 377–388 (2015).
40. Redza-Dutordoir, M. & Averill-Bates, D. A. Activation of apoptosis signalling pathways by reactive oxygen species. *Biochim Biophys. Acta* **1863**, 2977–2992 (2016).
41. Circu, M. L. & Aw, T. Y. Reactive oxygen species, cellular redox systems, and apoptosis. *Free Radic. Biol. Med.* **48**, 749–762 (2010).
42. Chai, P. et al. USP19 promotes hypoxia-induced mitochondrial division via FUNDC1 at ER-mitochondria contact sites. *J. cell Biol.* **220**, e202010006 (2021).
43. Lee, B. C., Kang, I. & Yu, K. R. Therapeutic Features and Updated Clinical Trials of Mesenchymal Stem Cell (MSC)-Derived Exosomes. *J. Clin. Med.* **10**, 711 (2021).
44. Yuan, Y. G. et al. Biogenesis, Composition and Potential Therapeutic Applications of Mesenchymal Stem Cells Derived Exosomes in Various Diseases. *Int J. Nanomed.* **18**, 3177–3210 (2023).
45. Pittenger, M. F. et al. Mesenchymal stem cell perspective: cell biology to clinical progress. *NPJ Regen. Med.* **4**, 22 (2019).
46. Rao, D. et al. Advances in Mesenchymal Stem Cell-Derived Exosomes as Drug Delivery Vehicles. *Front Bioeng. Biotechnol.* **9**, 797359 (2021).
47. Fan, X. L., Zhang, Y., Li, X. & Fu, Q. L. Mechanisms underlying the protective effects of mesenchymal stem cell-based therapy. *Cell Mol. Life Sci.* **77**, 2771–2794 (2020).
48. Wu, L. et al. Targeting Oxidative Stress and Inflammation to Prevent Ischemia-Reperfusion Injury. *Front Mol. Neurosci.* **13**, 28 (2020).
49. Granger, D. N. & Kvietys, P. R. Reperfusion injury and reactive oxygen species: The evolution of a concept. *Redox Biol.* **6**, 524–551 (2015).
50. Zhang, L., Dai, L. & Li, D. Mitophagy in neurological disorders. *J. Neuroinflamm.* **18**, 297 (2021).
51. Liu, L. et al. Mitophagy receptor FUNDC1 is regulated by PGC-1alpha/NRF1 to fine tune mitochondrial homeostasis. *EMBO Rep.* **22**, e50629 (2021).
52. Li, G., Li, J., Shao, R., Zhao, J. & Chen, M. FUNDC1: A Promising Mitophagy Regulator at the Mitochondria-Associated Membrane for Cardiovascular Diseases. *Front Cell Dev. Biol.* **9**, 788634 (2021).
53. Zhang, J. et al. Deubiquitinase USP35 restrains STING-mediated interferon signaling in ovarian cancer. *Cell death Differ.* **28**, 139–155 (2021).
54. Tang, Z. et al. Deubiquitinase USP35 modulates ferroptosis in lung cancer via targeting ferroportin. *Clin. Transl. Med.* **11**, e390 (2021).
55. Wang, W. et al. USP35 mitigates endoplasmic reticulum stress-induced apoptosis by stabilizing RRBP1 in non-small cell lung cancer. *Mol. Oncol.* **16**, 1572–1590 (2022).
56. Lin, G., Huang, T., Zhang, X. & Wang, G. Deubiquitinase USP35 stabilizes BRPF1 to activate mevalonate (MVA) metabolism during prostate tumorigenesis. *Cell death Discov.* **8**, 453 (2022).
57. Zhang, Q. et al. USP35 is a Potential Immunosuppressive Factor in Skin Cutaneous Melanoma. *J. Inflamm. Res.* **15**, 3065–3082 (2022).
58. Park, J., Kwon, M. S., Kim, E. E., Lee, H. & Song, E. J. USP35 regulates mitotic progression by modulating the stability of Aurora B. *Nat. Commun.* **9**, 688 (2018).
59. Wang, S. et al. The deubiquitylating enzyme USP35 restricts regulated cell death to promote survival of renal clear cell carcinoma. *Cell death Differ.* **30**, 1757–1770 (2023).
60. Merten, O. W., Hebben, M. & Bovolenta, C. Production of lentiviral vectors. *Mol. Ther. Methods Clin. Dev.* **3**, 16017 (2016).

Acknowledgements

This research was supported by the Zhejiang Provincial Natural Science Foundation of China (Grant No. LQ22H090020), the Zhejiang Provincial Science and Technology Plan of Traditional Chinese Medicine of China (Grant No. 2023ZR034), and the Zhejiang Provincial Medical Health Science and Technology Plan of China (Grant No. 2023RC012).

Author contributions

Conceptualization: S.W. and Y.J.; Methodology, X.L., S.W., and Y.J.; Investigation, X.L., T.W., Z.S., S.W., E.F., and Y.J.; Writing – Original Draft, S.W. and Y.J.; Writing –Review & Editing, X.L., T.W., Z.S., E.F., and Y.J.; Funding Acquisition, S.W.; Resources, T.W. and Z.S.; Supervision, S.W., E.F., and Y.J. All authors interpreted the data and edited the manuscript.

Competing interests

The authors declare no competing interests.

Additional information

Supplementary information The online version contains supplementary material available at https://doi.org/10.1038/s42003-024-07024-5.

Correspondence and requests for materials should be addressed to Yongming Jin.

Peer review information *Communications Biology* thanks Badrul Hisham Yahaya and the other, anonymous, reviewer(s) for their contribution to the peer review of this work. Primary Handling Editors: Toshiro Moroishi and David Favero.